Aalborg Universitet

A Modified Bi-Quad Filter Tuning Strategy for Mechanical Resonance Suppression in Industrial Servo Drive Systems

Chen, Yangyang; Yang, Ming; Sun, Yongping; Long, Jiang; Xu, Dianguo; Blaabjerg, Frede

IEEE POWER ELECTRONICS REGULAR PAPER/LETTER/CORRESPONDENCE

A Modified Bi-Quad Filter Tuning Strategy for Mechanical Resonance Suppression in Industrial Servo Drive Systems

Yangyang Chen, *Student Member, IEEE*, Ming Yang, *Senior Member, IEEE*, Yongping Sun, Jiang Long, Dianguo Xu, *Fellow, IEEE*, Frede Blaabjerg, *Fellow, IEEE*

Abstract—For mechanical resonance suppression, the bi-quad filter is a powerful tool and has been widely used in industrial applications. Compared with the notch filter, the bi-quad filter has one more parameter for notch depth design, which is more suitable for servo systems with nature damping coefficients and limited resonant gains. Usually, the bi-quad filter tuning has three steps, including identification, discretization, and switching process. However, in industrial applications, these three steps still have room for improvement. In this paper, three targeted modification methods are proposed. Firstly, an identification method based on the twins-point search is proposed to find out all of the available potential elastic characteristics accurately and quickly, and get the resonant frequency, the rejection bandwidth, and the notch depth for filter design. Then, inspired by the discretization distortion correction of the notch filter, a parameter mapping Tustin method is used to achieve accurate discretization. Furthermore, considering the bi-quad filter's settling time, a 'warm-up' buffer strategy prior to the filter switch-on is proposed to smooth the switching process. In the end, the validity and effectiveness of the proposed modification strategies are verified by experimental results.

Index Terms—Bi-quad filter, mechanical resonance, digital control, motor drive.

NOMENCLATURE

f_r, ω_r	Resonant frequency.
f_{ar}, ω_{ar}	Anti-resonant frequency.
f_{osc}	Oscillation frequency.
f_n, ω_n	Notch frequency of the notch filter.
b_n	-3 dB rejection bandwidth of the notch filter.
a_{1-2}	Notch filter factor.
Ω	Equivalent rejection bandwidth of the notch filter.
λ	Equivalent notch depth factor of the notch filter.
x_n	Notch filter rejection depth of $\omega_n \pm \Omega/2$.
f_b, ω_b	Notch frequency of the bi-quad filter.
f_{bd}	Real notch frequency of the bi-quad filter.
b_b	-3 dB rejection bandwidth of the notch filter.
x_b	Notch depth of the bi-quad filter.
k_{1-2}	Bi-quad filter characteristic coefficient.
b_{1-4}	Bi-quad filter factor.
T_s	Sampling period.
f_s	Sampling frequency.
f_{ASR}	Control frequency of the speed-loop.
k	Discretization time constant of Tustin.
k_W	Discretization time constant of pre-warped Tustin.
k_Z	Zero-pole matching discretization gain.
ω_0	Start frequency of the twins-point search.
ω_1	Obtained anti-resonant frequency.
ω_2	Obtained resonant frequency.
ω_3	Termination frequency of the twins-point search.
$m(f)$	Magnitude of the frequency f.
ζ	Damping coefficient of the bi-quad filter.
ω_{bd}	Equivalent vibration frequency of the bi-quad filter.
T_b	Equivalent settling time of the bi-quad filter.
W	Warm-up period of the bi-quad filter.
q_1	Twins-point search magnitude threshold.
q_2	Twins-point search bandwidth threshold.
q_3	Twins-point search effectiveness threshold.
q_4	Twins-point search notch bandwidth factor.
q_5	Twins-point search notch depth factor.
f_{sc}	Expected speed loop bandwidth.
$.^*$	Mapped filter parameter.
$._P$	Percentage error.
Δ	Symbol of error and variation.

I. INTRODUCTION

Nowadays, the improvement of servo systems has brought significant changes and benefits to the modern industry. A series of controller tuning methods to maximize existing equipment's productivity have been proposed [1], [2]. The most direct way to improve machines' efficiency is to increase the controller gain, but the higher controller gain may cause other problems, like the mechanical resonance. In most servo systems, elastic transmission equipments have potential resonance characteristics [3], [4]. The mechanical resonance in

IEEE POWER ELECTRONICS REGULAR PAPER/LETTER/CORRESPONDENCE

servo systems with elastic couplings is an obstacle for users to increase controller gain and improve production efficiency.

To solve this problem, many classic theories, including optimal control, Kalman filter, Luenberger observer, and so on, have been successfully applied to servo systems [5]–[12]. However, in general, filtering is still one of the most straightforward solutions, and it is widely used in industrial and commercial production [3], [4], [13]–[31], and its related algorithms are improved continuously. In [3] and [4], the typical notch filter and bi-quad filter for the two-mass mechanical system have been comprehensively discussed. Usually, the on-line fast Fourier transform (FFT) is preferred in servo systems for resonant frequency ω_r identification and filter tuning [14]. Kang *et al.* [15] used a shifted structure to achieve real-time detection of mechanical resonance information. In [16], a modified speed measurement method is introduced for removing a dominant noise cluster in the FFT spectrum. Following identification, a modified notch filter with a smaller additional phase shift and better ability to attenuate high-frequency vibrations is proposed in [17]. For power grids, the problems of harmonics and resonances also exist [18]-[24]. As for the compensation of the harmonics, the second-order generalized integrator (SOGI) based adaptive notch filter (ANF) has been widely used to extract in-quadrature signals of desired frequency [18]-[21]. Dislike the harmonics compensation, the target of the *LCL* filter resonance damping in power grids is different. It aims to reduce the potentially unstable dynamics and improve the stability of the *LCL*-filter-based grid-connected converters through active or passive damping methods [22]-[24], which is a more similar problem with mechanical resonance suppression.

Overall, there are three steps in the filter strategy, resonance frequency identification, filter discretization, and filter switch-on process. As for the resonant frequency ω_r identification based on FFT analysis, there are two types of methods: on-line and off-line. Usually, in the past decade, adjustable on-line FFT analysis mentioned above [19]–[16] is more prevalent in universal servo systems. In a system with elastic couplings, the 'resonant' frequency f_r is the frequency of the gain peak caused by the elastic coupling. The 'oscillation' frequency f_{osc} is the frequency obtained by the on-line method when the system is unstable. However, strictly, 'oscillation' frequency is not equal to 'resonant' frequency. Adding a filter with the notch frequency as the 'oscillation' frequency will even cause a severer oscillation, which is discussed comprehensively in [25]-[27]. This phenomenon is called 'oscillation frequency deviation'. In [25], a self-tuning low-pass filter is used to enhance the performance of the on-line method and so that the deviation is attenuated. Besides, the influencing factors of the deviation are analyzed in [26] and [27]. This phenomenon is shown in **Fig. 1**, where the step response of a typical two-mass system contains a 'resonance'. In this situation, when on-line methods are applied, the steady-state signal with oscillation frequency f_{osc2} is used for resonance frequency identification. Then, the identification result f_{osc2} is chosen as the notch frequency f_n of the notch filter. However, after adding a notch
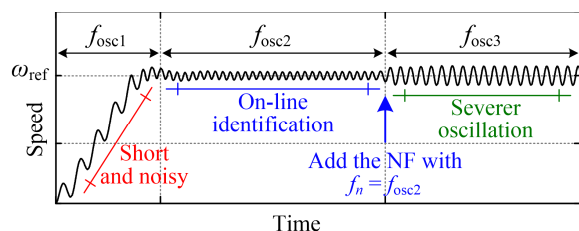

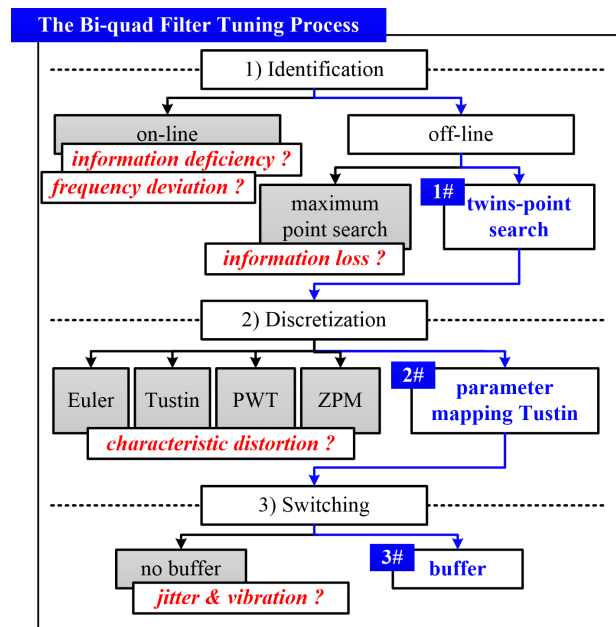Fig. 1. The oscillation frequency deviation in servo drive systems.

Fig. 2. The flow chart and the design intention of the filter tuning strategy.

filter, the system's oscillation becomes severer, and the oscillation frequency is changed to f_{osc3}. Thus, when the deviation happens, the on-line identification result is wrong, and the steps to correct this deviation will be relatively complex. More details will be discussed in Part II and be verified by the experiment results of Part V. Today, for those machines with commissioning processes, higher damping, smaller control delay, and higher bandwidth, the classic off-line resonant frequency identification [28]–[31] is more suitable. Then, how to make full use of the information from the FFT analysis result and how to get rid of the impact of the noise are still open problems.

When the system's resonant frequency is obtained, both the notch filter and the bi-quad filter can be good candidates to filter out the resonant frequency signal with the resulting influence to other frequency bands as small as possible [3]. Compared with the notch filter, the bi-quad filter has one more parameter to adjust the notch depth of the central notch frequency. Because of the natural damping coefficient, the magnitude of the industrial system's resonance frequency is not infinity. Hence, the bi-quad filter is more suitable. Next, filter discretization is necessary before the implementation of the filter. However, this discretization process will cause the characteristic distortion of the bi-quad filter, like the deviation of the notch frequency and the narrowing of the notch width, which is similar to the case of notch filters [27], [32]. When

IEEE POWER ELECTRONICS REGULAR PAPER/LETTER/CORRESPONDENCE

the system's natural resonance frequency is higher, adding a distorted digital bi-quad filter cannot stabilize the system. It means the bi-quad filter does not have the effect as it is designed for.

Besides the identification and the discretization, the time of filter switching is another part that can be improved. Because the initial values of filter variables are zero (or uncertain values), to some extent, the output of an empty filter actually can be regarded as a step response at the beginning, which will cause jitter and vibration of the filter output torque.

In this paper, as shown in **Fig. 2**, three targeted modifications on the classic bi-quad filter are proposed in this paper. Firstly, by analyzing the disadvantages of the conventional maximum point search based resonant frequency identification, a twins-point search concept is built up. The twins-point search can successfully reduce the noise's impact and fully describe the system's entire multi-mass characteristic. Then, the characteristic distortion problems of the classic Tustin, pre-warped Tustin (PWT), and zero-pole matching (ZPM) methods are discussed. By referring to the notch filter's discretization correction process, a bi-quad filter parameter mapping Tustin (PMT) strategy is proposed to make it work effectively. Besides, because the sudden switching will impact the system's stability, an easy-to-implement buffer strategy is introduced. The proposed strategy's effectiveness and advantages are verified on a 750 W motor drive platform with elastic couplings.

II. Off-Line Resonant Frequency Identification Based on Twins-Point Search

A. The On-Line Resonant Frequency Identification and the Oscillation Frequency Deviation Phenomenon

In many industrial applications, the on-line resonant frequency identification based on the FFT analysis or the ANF is preferred. In detail, based on the methods mentioned above, the so-called dominant 'resonant frequency' is acquired and then used to tuning the bi-quad filter. Although the notch frequency can be obtained, the last parameters of filters, like the rejection bandwidth and the notch depth, cannot be obtained directly from these methods. Moreover, the 'oscillation' frequency f_{osc} cannot be regarded as the real 'resonant' frequency f_r; if not, the wrong notch frequency will lead to the filter's failure. Actually, because of the saturation nonlinearity of the speed controller's output, the 'oscillation' frequency is the $-\pi$ cross-over frequency of the system's open-loop bode diagram, which can be much higher than the real 'resonant' frequency [25]-[27]. As shown in **Fig. 3**, with the technology development (the red line: higher control frequency, the green line: smaller control delay in the current loop), the phase-lag of common servo systems becomes smaller (a high damping coefficient can also lead to this problem), and the $-\pi$ cross-over frequency of the open-loop transfer function moves from the resonant frequency f_r (the blue line) to a higher frequency.

In **Fig. 4**, the $-\pi$ cross-over 'oscillation' frequency of the original system (the blue line) is higher than the 'resonant'
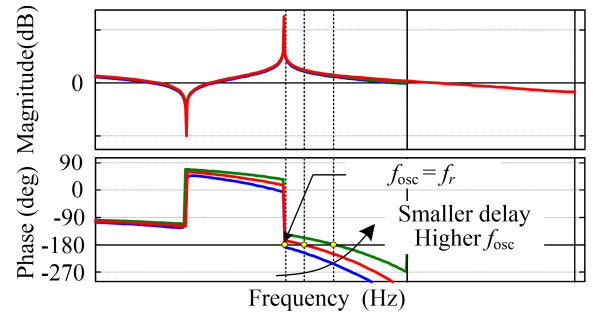

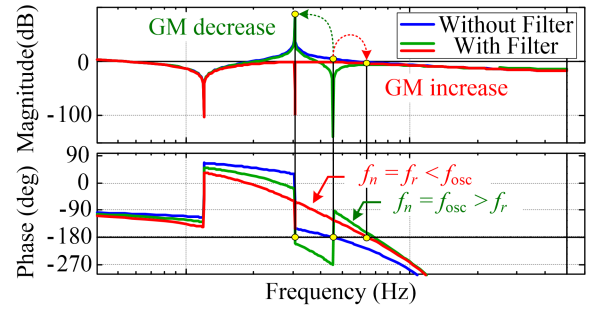Fig. 3. The open-loop Bode diagram of digital two-mass servo systems.

Fig. 4. The effects of notch filters with different types of notch frequencies when the frequency deviation happens.

frequency (the peak frequency of the magnitude). If chosen the $-\pi$ cross-over 'oscillation' frequency f_{osc} as the notch frequency f_n, (the green line), the $-\pi$ cross-over frequency will become closer to the resonant frequency, and the gain margin (GM) of the system will be even worse. However, if f_n is the real 'resonant' frequency f_r (the red line), the correct notch filter will reduce the peak magnitude and compensate for the phase delay. Hence, the $-\pi$ cross-over frequency of the red line is pushed to a higher frequency, and the GM of the system becomes better. Nowadays, since the control frequency and the current loop bandwidth become much higher than before, rather than the resonance, the oscillation caused by unsuitable controller gain is more common in modern servo systems. When the oscillation happens, the wrong resonant frequency obtained by conventional on-line resonant frequency identification methods may lead to the filter's failure and even make the oscillation worse.

In general, the major problem of the on-line method is information deficiency. Many reasons, including resonance, oscillation frequency deviation, potential multi-resonance characteristics (more than two-mass), or even the rigid system's excessive control gain, can lead to instability. A dominant narrow cluster from the frequency spectrum is not enough to tune the bi-quad filter parameters directly, and hard to make a comprehensive judgment about the system's state.

B. The Off-line Twins-Point Search

As mentioned above, the off-line identification method is more suitable in those situations with relatively fixed mechanical structures and characteristics, like numerical controlled machine tools. Additionally, a short off-line

commissioning process is acceptable, and it will not impact the regular operation of the on-line method.

However, the off-line method still has room for improvement. Because of the limited computing power and storage space of the industrial control chip, users will prefer to use the simplest combination of the FFT analysis and the maximum point search in industrial applications. The shortcomings of the conventional maximum point search are shown in **Fig. 5** and listed as follows.

1) Some resonant details are ignored (the blue line, more than two-mass), and the algorithm cannot directly obtain the notch bandwidth and depth factors.

2) As for the red line, the magnitude of the low frequency is higher. If the start frequency is unsuitable, the maximum point search gets the wrong resonant frequency.

Hence, a more comprehensive resonant frequency search method without adding enormous computing burden and storage space is needed. According to the analysis of the multi-mass model, the resonant point does not exist independently. Besides the resonant frequency, there is another unique frequency called 'anti-resonant frequency' f_{ar}. The resonant frequency has the maximum magnitude among the nearby bandwidth, but the anti-resonant point has the minimum gain. Based on the characteristic of the 'twins-point' (the resonant and the anti-resonant frequencies), a twins-point search is proposed and shown in **Fig. 6**. Because of the special location mode in the twins-point search, this method can effectively avoid the wrong choice of the resonant frequency and information loss.

Some detailed procedures of the twins-point search are designed as follows. In a real system, the problem of noise is unavoidable. Therefore, in **Fig. 7**, the noise in the FFT analysis result is taken into consideration, and the principle of twins-point search can be expressed as

$$\begin{cases} \omega_0 < \omega_1 < \omega_2 < \omega_3 \\ m(\omega_1) = \min\{m(\omega)|\omega \in [\omega_0, \omega_3]\} \\ m(\omega_2) = \max\{m(\omega)|\omega \in [\omega_1, \omega_3]\} \\ [m(\omega_2) - m(\omega_3)]/[m(\omega_2) - m(\omega_1)] \geq q_1 \\ \omega_3 - \omega_2 \geq q_2 \end{cases} \quad (1)$$

in which ω_0 and ω_3 are the start frequency and termination frequency of each twins-point search; ω_1 and ω_2 are the obtained anti-resonant frequency and resonant frequency; $m(\omega)$ is the magnitude of the frequency ω without logarithmic operation; q_1, q_2, and q_3 are threshold coefficients.

Each time (1) is satisfied, the current twins-point search is finished, and the next turn of the search begins. However, not all of the obtained twins-points are qualified. One last constraint is needed, and it is given as

$$m(\omega_2)/m(\omega_1) > q_3 \quad (2)$$

Based on the (1) and (2), the structure of an easy-implemented twins-point search method can be built up. Owing to the twins-point search's characteristic, no wrong choice of resonant frequency and resonant information loss will happen in most situations. Then, the information from (1)
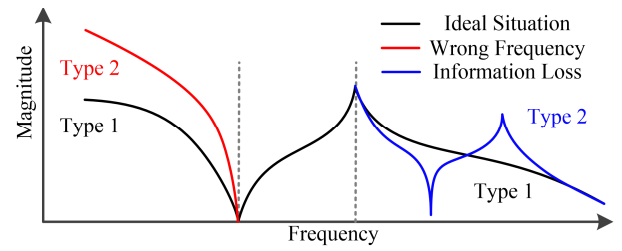

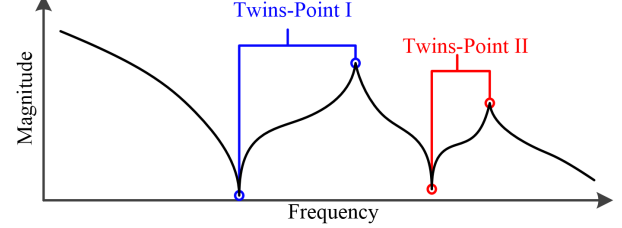Fig. 5. The shortcomings of the maximum point search.

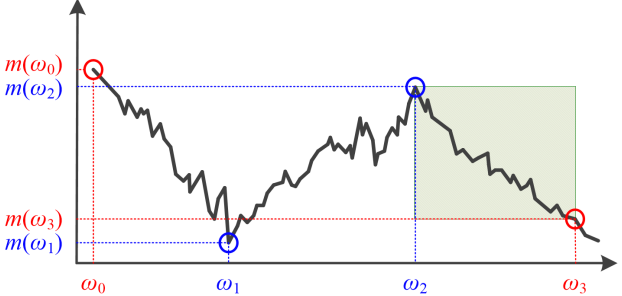Fig. 6. The twins-point search diagram.

Fig. 7. The principle of the twins-point search.

can be used for the parameter choice of the filter. A set of empirical formulas is given as

$$\begin{cases} \omega_b = \omega_2 \\ b_b = q_4 (\omega_2 - \omega_1) \\ x_b = 20 q_5 \log(0.5[m(\omega_2) + m(\omega_1)]/m(\omega_2)) \end{cases} \quad (3)$$

in which, ω_b is the notch frequency; b_b is the rejection bandwidth of -3 dB; x_b is the notch depth, q_4 and q_5 are the manual tuning factors to meet the different requirements of the users (more stable or less influence from the filter).

In detail, the bi-quad filter has two functions. The first one is to reduce the peak gain of the resonant frequency $m(\omega_2)$. Here, the average value of $m(\omega_1)$ and $m(\omega_2)$, then divided by $m(\omega_2)$, is selected as the reference notch depth value. The second function is to dig the phase margin between the anti-resonant frequency f_{ar} and the resonant frequency f_r (as shown in **Fig. 4**) to compensate for the phase lag of the frequency band after f_r. Thus, the width from f_{ar} to f_r can be selected as half of the -3 dB rejection bandwidth standard value.

III. PROPOSED PARAMETER MAPPING TUSTIN METHOD

A. The Classic Notch Filter and the Bi-Quad Filter

Fig. 8 shows the magnitude-frequency characteristic, the phase-frequency characteristic, and the group-delay of the notch filter and the bi-quad filter, in which ω_n and ω_b are the notch frequencies of the notch filter and the bi-quad filter

respectively, and b_n and b_b represent the -3 dB rejection bandwidth, and x_b is the notch depth of the bi-quad filter. Compared with the notch filter, the bi-quad filter is more flexible, and it has a better group-delay characteristic. Because the entire system is a closed-loop control system and not a one-way signal transmission channel, the group-delay characteristic will not be discussed in-depth. Additionally, an appropriate phase distortion of the filter (with correct notch frequency) can be superimposed on the original system and improve the system's stability, as shown in **Fig. 4**.

1) Notch Filter

From **Fig. 8**, the classic transfer function of the widely used notch filter can be given as

$$G_n(s) = \frac{s^2 + \omega_n^2}{s^2 + b_n s + \omega_n^2} \tag{4}$$

where, ω_n is the notch frequency, and b_n is the -3 dB rejection bandwidth. Usually, ω_n is selected to approximate the resonance frequency of the servo drive systems.

Applying Tustin transformation to discretize (4) yields

$$G_n(z) = G_n(s)\big|_{s=k\frac{z-1}{z+1}}$$
$$= \frac{(k^2 + \omega_n^2) - 2(k^2 - \omega_n^2)z^{-1} + (k^2 + \omega_n^2)z^{-2}}{(k^2 + \omega_n^2 + kb_n) - 2(k^2 - \omega_n^2)z^{-1} + (k^2 + \omega_n^2 - kb_n)z^{-2}} \tag{5}$$

in which $k = 2/T_s$ and T_s is the sampling period.

Assuming a_1 and a_2 are notch filter factors, and they can be expressed as

$$\begin{cases} a_1 = \dfrac{2(k^2 - \omega_n^2)}{k^2 + \omega_n^2 + kb_n} \\ a_2 = \dfrac{k^2 + \omega_n^2 - kb_n}{k^2 + \omega_n^2 + kb_n} \end{cases} \tag{6}$$

Then, the simplified transfer function of the notch filter in z-domain (5) can be given as

$$G_n(z) = \frac{1}{2} \cdot \frac{(1 + a_2) - 2a_1 z^{-1} + (1 + a_2)z^{-2}}{1 - a_1 z^{-1} + a_2 z^{-2}} \tag{7}$$

However, (7) does not consider the negative effect of the Tustin transformation. In other words, the transformation will cause the deviation of the notch frequency and weaken the notch depth. Hence, the Direct-Form II transposed (DFIIt) structure [24], [32] is used to do further modification of (5), and the notch filter can be rewritten as

$$G_n(e^{j\omega T_s}) = \frac{(k^2 + \omega_n^2)\cos(\omega T_s) - (k^2 - \omega_n^2)}{(k^2 + \omega_n^2)\cos(\omega T_s) - (k^2 - \omega_n^2) + jkb_n\sin(\omega T_s)} \tag{8}$$

Then magnitude of (8) can be calculated by solving

$$\left((k^2 + \omega_n^2)\cos(\omega T_s) - (k^2 - \omega_n^2)\right)^2 \lambda^2 = k^2 b_n^2 \sin^2(\omega T_s) \tag{9}$$

in which λ can be expressed as (Ω is the rejection bandwidth and the magnitude of the notch filter at $\omega_n \pm \Omega/2$ is x_n dB)

$$|\lambda| = \sqrt{10^{-x_n/10} - 1} \tag{10}$$

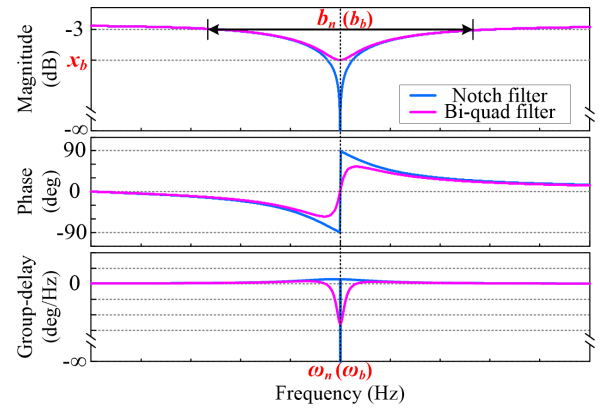Substituting $\omega = \omega_n \pm \Omega/2$ into (9) yields

Fig. 8. The notch and the bi-quad filters' parameters definition.

$$\Omega T_s = \arccos \frac{\lambda^2 (k^2 + \omega_n^2)^2 - k^2 b_n^2}{\lambda^2 (k^2 + \omega_n^2)^2 + k^2 b_n^2} \tag{11}$$

which will result in the magnitude of (8) to be x_n dB.

From (9), the coefficient b_n can be calculated as

$$b_n = \frac{\lambda}{k}\left(k^2 + \tan^2\left(\frac{\omega_n T_s}{2}\right)\right)\tan\left(\frac{\Omega T_s}{2}\right) \tag{12}$$

Then, a_1 and a_2 of the notch filter can be rewritten as

$$\begin{cases} a_1 = \dfrac{2\cos(\omega_n T_s)}{1 + \lambda \cdot \tan(\Omega T_s/2)} \\ a_2 = \dfrac{1 - \lambda \cdot \tan(\Omega T_s/2)}{1 + \lambda \cdot \tan(\Omega T_s/2)} \end{cases} \tag{13}$$

2) Bi-Quad Filter

From **Fig. 8**, compared with the notch filter, the bi-quad filter can adjust the notch depth x_b of its notch frequency ω_b. The transfer function of the bi-quad filter can be given as

$$G_b(s) = \frac{s^2 + k_2 \omega_b s + \omega_b^2}{s^2 + k_1 \omega_b s + \omega_b^2} \tag{14}$$

The bi-quad filter coefficients k_1 and k_2 can be calculated as

$$\begin{cases} k_1 = b_b/\omega_b \\ k_2 = 10^{x_b/20} \cdot b_b/\omega_b \end{cases} \tag{15}$$

where ω_b is the notch frequency, b_b is the -3 dB rejection bandwidth, and the bi-quad filter magnitude at ω_b is x_b dB.

Applying Tustin transformation to discretize (14) yields

$$G_b(z) = G_b(s)\big|_{s=k\frac{z-1}{z+1}} = \frac{(b_1 + b_4) + b_2 z^{-1} + (b_1 - b_4)z^{-2}}{(b_1 + b_3) + b_2 z^{-1} + (b_1 - b_3)z^{-2}} \tag{16}$$

in which, b_1, b_2, b_3, and b_4 are the bi-quad filter factors

$$\begin{cases} b_1 = T_s^2 + 4/\omega_b^2 \\ b_2 = 2(T_s^2 - 4/\omega_b^2) \\ b_3 = 2b_b T_s/\omega_b^2 \\ b_4 = 2b_b 10^{x_b/20} T_s/\omega_b^2 \end{cases} \tag{17}$$

Different from the notch filter, the bi-quad filter has three adjustable parameters. The DFIIt structure cannot be used to

modify the transfer function of the bi-quad filter in the z-domain (16). Hence, when ω_b is higher or close to the Nyquist frequency $1/(2T_s)$, the bi-quad filter's discrete characteristics will deviate from the expectation.

The pre-warped Tustin (PWT) and zero-pole matching (ZPM) discretization methods are two classic solutions for this problem, but they still have their shortcomings.

The PWT discretization process can be expressed as

$$G_b(z) = G_b(s)\Big|_{s=k_W \cdot \frac{z-1}{z+1}} \quad (18)$$

in which, based on the notch frequency ω_b of the bi-quad filter, the PWT factor k_W can be expressed as

$$k_W = \omega_b / \tan(\omega_b T_s / 2) \quad (19)$$

Although the PWT can fix the distortion of the notch frequency ω_b, the -3 dB rejection bandwidth b_b after the discretization is still narrowed.

As for the ZPM method, through the polynomial factorization, $G_b(s)$ can be rewritten as

$$G_b(s) = \frac{(s+z_1)(s+z_2)}{(s+p_1)(s+p_2)} \quad (20)$$

in which, z_1, z_2, p_1, and p_2 are zeros and poles of $G_b(s)$.

Then, the ZPM based discretization bi-quad filter can be expressed as

$$G_b(z) = \frac{k_Z\left(z-e^{-z_1 T_s}\right)\left(z-e^{-z_2 T_s}\right)}{\left(z-e^{-p_1 T_s}\right)\left(z-e^{-p_2 T_s}\right)} \quad (21)$$

where, the discretization gain k_Z can be calculated as

$$G_b(s)\Big|_{s=0} = G_b(z)\Big|_{z=1} \quad (22)$$

Compared with the PWT method, the ZPM can achieve better discretization performance in the controller gain. However, it also leads to a larger phase delay, and its calculation process is more complicated.

The comparison results of all the discretization methods mentioned above will be given in the following analysis.

B. The Discretization Distortion Model

According to the analysis above, the notch filter can fix the distortion caused by discretization, but its notch depth is infinity. Although the bi-quad filter can adjust the notch depth at the central notch frequency, the discretization distortion is an obstacle for a bi-quad filter to cope with the resonance with higher frequencies. In this part, a parameter mapping Tustin discretization (PMT) method for the bi-quad filter is proposed to combine the advantages of these two kinds of filters. By reviewing the modification of the notch filter, a different derivation process can be obtained from the parameter mapping perspective. Let the numerator in (8) be zero, when the notch frequency is still ω_n in the z-domain, the formulation of the corrected notch frequency factor ω_n^* can be given as

$$\left(k^2 + \omega_n^{*2}\right)\cos \omega_n T_s - \left(k^2 - \omega_n^{*2}\right) = 0 \quad (23)$$

Because $\omega_n^* > 0$, ω_n^* can be expressed as

$$\omega_n^* = \frac{2}{T_s}\sqrt{\frac{1-\cos \omega_n T_s}{1+\cos \omega_n T_s}} \quad (24)$$

By substituting (24) into (8), the phase of (8) with ω_n^* can be given as

$$\angle G_n\left(e^{j\omega T_s}\right) = \arctan \frac{kb_n \sin \omega T_s}{\left(k^2 + \omega_n^{*2}\right)\cos \omega T_s - \left(k^2 - \omega_n^{*2}\right)} \quad (25)$$

According to the Shannon theorem $\omega T_s < \pi$, the phase of (25) around ω_n can be given as

$$\begin{cases} \angle G_n\left(e^{j\omega_{n-} T_s}\right) = \arctan \dfrac{b_n\left(1+\cos \omega_n T_s\right)\sin \omega_{n-} T_s}{2k\left(\cos \omega_{n-} T_s - \cos \omega_n T_s\right)} = -\dfrac{\pi}{2} \\[3mm] \angle G_n\left(e^{j\omega_{n+} T_s}\right) = \arctan \dfrac{b_n\left(1+\cos \omega_n T_s\right)\sin \omega_{n+} T_s}{2k\left(\cos \omega_{n+} T_s - \cos \omega_n T_s\right)} = +\dfrac{\pi}{2} \end{cases} \quad (26)$$

Furthermore, to modify the rejection bandwidth factor, constructing the following equation

$$\left\{\left(k^2 + \omega_n^{*2}\right)\cos \omega T_s - \left(k^2 - \omega_n^{*2}\right)\right\}^2 \lambda^2 = k^2 b_n^2 \sin^2 \omega T_s \quad (27)$$

By substituting (27) and (10) into (8), the magnitude of (8) can be calculated as

$$20\lg\left|\frac{Q}{Q+j\lambda Q}\right| = 20\lg\left|\frac{1}{1+j\lambda}\right| = 20\lg\left|\frac{1}{1+j\lambda}\right| = x_n \quad (28)$$

where Q can be expressed as

$$Q = \left(k^2 + \omega_n^{*2}\right)\cos \omega_n T_s - \left(k^2 - \omega_n^{*2}\right) \quad (29)$$

According to (28), when (27) and (10) are valid, the magnitude of (8) at ω is x_n. Assuming when the -3 dB rejection bandwidth is still b_n in z-domain, the corrected notch bandwidth factor is b_n^*. Considering the results of the trigonometric functions, by substituting $\omega = \omega_n - b_n/2$ or $\omega = \omega_n + b_n/2$ into (27), the expression of b_n^* can be given as

$$b_n^* = \begin{cases} \left|\dfrac{\lambda\left\{\left(k^2+\omega_n^{*2}\right)\cos\left[\left(\omega_n+b_n/2\right)T_s\right]-\left(k^2-\omega_n^{*2}\right)\right\}}{k\sin\left[\left(\omega_n+b_n/2\right)T_s\right]}\right|, \omega_n \le \dfrac{\pi f s}{2} \\[4mm] \left|\dfrac{\lambda\left\{\left(k^2+\omega_n^{*2}\right)\cos\left[\left(\omega_n-b_n/2\right)T_s\right]-\left(k^2-\omega_n^{*2}\right)\right\}}{k\sin\left[\left(\omega_n-b_n/2\right)T_s\right]}\right|, \omega_n > \dfrac{\pi f s}{2} \end{cases} \quad (30)$$

C. The Bi-Quad Filter Accurate Discretization Strategy

Because the notch filter and the bi-quad filter have some similarities in their structures and parameters, the mapping equations (24) and (30) can also modify the notch frequency and bandwidth factors of the bi-quad filter and weaken the discretization effect.

Hence, (17) can be rewritten as

$$\begin{cases} b_1 = T_s^2 + 4/\omega_b^{*2} \\[2mm] b_2 = 2\left(T_s^2 - 4/\omega_b^{*2}\right) \\[2mm] b_3 = 2b_b^* T_s/\omega_b^{*2} \\[2mm] b_4 = 2b_b^* 10^{x_b/20} T_s/\omega_b^{*2} \end{cases} \quad (31)$$

The performance of the bi-quad parameter correction is shown in **Fig. 9**, in which $\omega_b = 2\pi \times 800$ rad/s, $b_b = \omega_b = 2\pi \times 800$ rad/s, $x_b = -30$ dB, and $T_s = $ 5e-4 s. From **Fig. 9**, by applying (24) and (30), compared with Tustin, PWT and ZPM, the characteristic distortion caused by discretization is significantly weakened by using the proposed PMT.
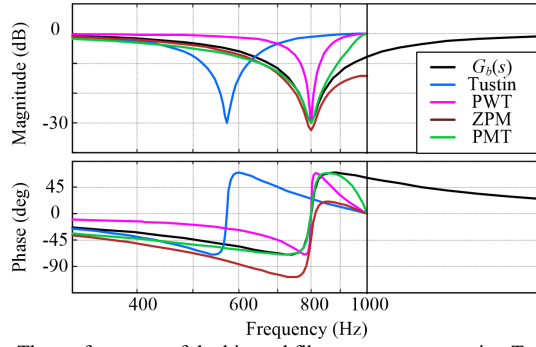
IEEE POWER ELECTRONICS REGULAR PAPER/LETTER/CORRESPONDENCE

Fig. 9. The performance of the bi-quad filter parameter mapping Tustin when $\omega_b = b_b = 2\pi \times 800$ rad/s, $x_b = -30$ dB, and $T_s = $ 5e-4 s.

Additionally, a set of comparison results is recorded to show the advantage of the proposed PMT method. As shown in **Fig. 10**, three evaluation functions are given as

$$\Delta f_{bP} = (f_b - f_{bd})/f_b \qquad (32)$$

$$\Delta b_P = \Delta b / (b_b/2) \qquad (33)$$

$$\Delta P_P = \frac{\int_{\omega_b - b_b/2}^{\omega_b + b_b/2} \left| \angle G_b(s) - \angle G_b(z) \right| d\omega}{\int_{\omega_b - b_b/2}^{\omega_b + b_b/2} \left| \angle G_b(s) \right| d\omega} \qquad (34)$$

in which, $f_b = \omega_b/(2\pi)$, and f_{bd} is the real notch frequency after the discretization, Δf_{bP} from (32) represents the notch frequency distortion, while Δb_P from (33) and ΔP_P from (34) are the magnitude-characteristic and the phase-characteristic distortion indexes respectively. In practice, for (34), the discrete summation (the discrete step is 0.1 Hz) is used to replace the continuous integral in this paper.

Fig. 11, **Fig. 12**, and **Fig. 13** show the comparison results of Tustin, PWT, ZPM, and PMT based on indexes (32)-(34) under different notch frequencies f_b (all of the filters have -3 dB rejection bandwidth $b_b = \omega_b$, notch depth $x_b = -30$ dB, discretization period $T_s = $ 5e-4 s, discretization frequency $f_s = $ 2000 Hz).

First, in **Fig. 11**, the notch frequency distortion Δf_{bP} of the Tustin method increases to larger than 30% when the expected notch frequency f_b reaches 850 Hz. Additionally, the notch frequency of ZPM slightly deviates when f_b increases to 700 Hz. However, the distortions of PWT and PMT are eliminated.

Next, in **Fig. 12**, the ZPM has the best performance in the test of magnitude-characteristic distortion, and both the distortion range of ZPM and the proposed PMT is within $\pm$ 30% (a further discussion about this 'notch bandwidth deviation' phenomenon will be given in the next part). In contrast, following the increase of f_b, the notch bandwidth of PWT shrinks significantly.

As for the phase distortion in **Fig. 13**, when f_b is smaller than 250 Hz, the ΔP_P of PMT is slightly larger than PWT and ZPM. However, from 250 Hz to 900 Hz, the distortion of PWT and ZPM increases dramatically, while the proposed PMT method still has good performance under different notch depth and notch frequency ($\Delta P_P < 20\%$). When $f_b = 900$ Hz, ΔP_P of PWT is larger than 60%, and ΔP_P of ZPM is even more than 80%. Especially, as shown in **Fig. 9**, the ZPM has the largest-phase delay in this situation.
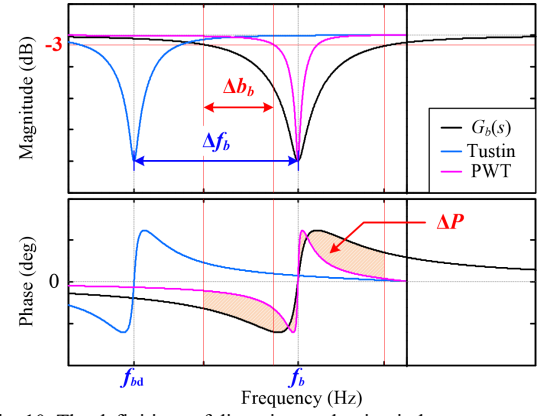

Fig. 10. The definitions of distortion evaluation indexes.
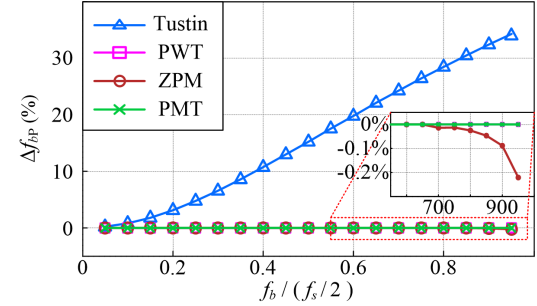

Fig. 11. The notch frequency distortion after the discretization.
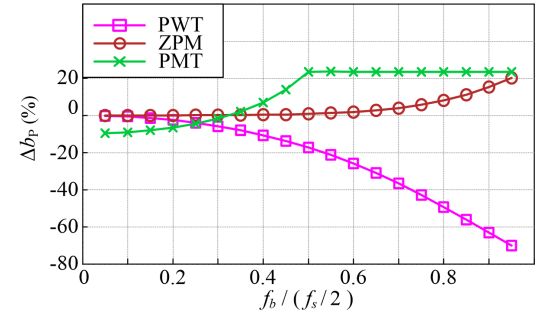
Fig. 12. The magnitude-characteristic distortion after the discretization.
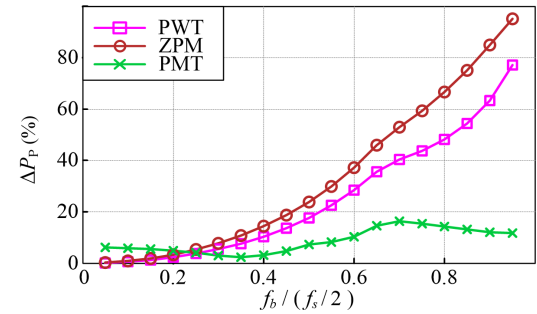
Fig. 13. The phase-characteristic distortion after the discretization.

In conclusion, the proposed PMT method has a good performance in the bi-quad filter discretization. Although the classic PWT method can cope with the notch frequency distortion, it cannot handle the characteristic of other frequency range, which is away from the notch frequency ω_b. This problem can lead to the narrowing of the -3 dB rejection bandwidth b_b and the distortion of the phase compensation. The ZPM method can keep the discretization accuracy of the

filter gain, but it causes additional phase-delay and then decreases the bi-quad filter's anti-resonance ability after discretization.

D. The Notch Bandwidth Deviation Phenomenon

In many industrial applications, the bi-quad filter design will use the conclusion that $|G(\omega_b-b_b/2)|$ = -3 dB, but this equation is not correct in some situations. The gain of the bi-quad filter $G_b(\omega)$ can be approximately calculated as

$$\left|G_b\left(\omega\right)\right| \approx \sqrt{\left(\omega_b^2 - \omega^2\right)^2 \Big/ \left[\left(\omega_b^2 - \omega^2\right)^2 + b_b^2\omega^2\right]} \qquad (35)$$

Then, setting $\omega = \omega_b - b_b/2$ and $q = b_b/\omega_b$, (35) can be rewritten as

$$\left|G_b\left(\omega_b - b_b/2\right)\right| = \left|G_b\left(\left(1-q/2\right)\omega_b\right)\right|_{q=b_b/\omega_b}$$
$$\approx \sqrt{\left(q-4\right)^2 \Big/ \left(5q^2 - 24q + 32\right)} \qquad (36)$$

Because (36) is a monotonically increasing function in $q \in$ (0, 2), the damping ability of the bi-quad filter at $\omega_b-b_b/2$ will decrease following with the increasing of the b_b/ω_b. This notch bandwidth deviation phenomenon is shown in **Fig. 14**, in which the values of the bi-quad filter parameters is same with the values in the experiments of Part V ($\omega_b = 2\pi\times167$ rad/s, $b_b = 2\pi\times280$ rad/s, x_b = -29 dB, and T_s = 2e-3 s). Additionally, for better verification, setting the notch bandwidth deviation index Δb_{PH} as

$$\Delta b_{PH} = \left(b_d - b_b/2\right)\Big/\left(b_b/2\right) \qquad (37)$$

in which b_d is the real -3 dB rejection bandwidth on the left side of the notch frequency ω_b.

As for different bi-quad filters (both continuous and discrete), their relationships between Δb_{PH} and b_b/ω_b are shown in **Fig. 15**. According to **Fig. 14** and **Fig. 15**, the left side -3 dB notch bandwidths of the continuous bi-quad filter and the ZPM based bi-quad filter decrease with the increase of b_b/ω_b ($0 < b_b/\omega_b < 2$). In contrast, the proposed PMT method does not have this deviation trend. Because one of the aims of the bi-quad filter and the proposed twins-point search method is to use the phase margin from the anti-resonant frequency to the resonant frequency, the accuracy design and execution of the -3 dB rejection bandwidth on the left side of ω_b are important. Hence, in this situation, the PMT method can be a better choice than the classic ZPM method, and the parameter calculation process of the PMT method is also simpler.

IV. BUFFER STRATEGY OF BI-QUAD FILTER SWITCHING

Usually, in many self-tuning filter strategies, the switching or the on-off process of filters is unbuffered. However, when the input signal has a relatively large offset, adding a filter into the original system will cause an abrupt change of the control signal. For example, as for motor drive systems, there will be an offset current in the q-axis to cancel out external disturbances because of the damping and the load torque. The sudden output electromagnetic torque distortion caused by the turn-on of the bi-quad filter can cause the vibrations of output torque and motor speed. Hence, a buffer strategy is necessary. A simple solution to this problem is to prepare a short buffer
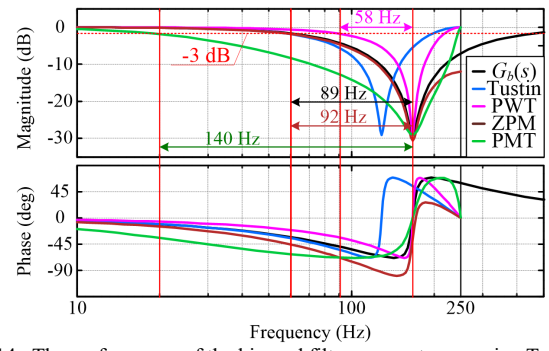

Fig. 14. The performance of the bi-quad filter parameter mapping Tustin when $\omega_b = 2\pi\times167$ rad/s, $b_b = 2\pi\times280$ rad/s, x_b = -29 dB, and T_s = 2e-3 s.
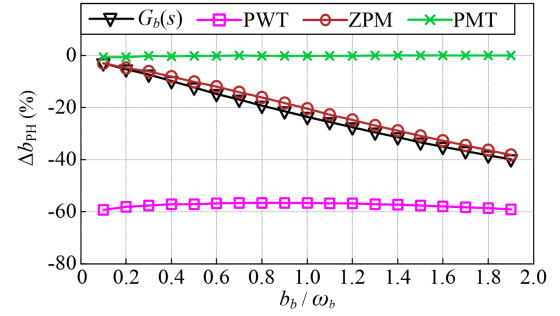

Fig. 15. The notch bandwidth deviation comparison results ($\omega_b = 2\pi\times167$ rad/s, x_b = -30 dB, and T_s = 2e-3 s).
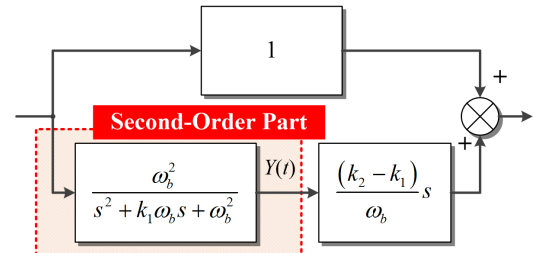

Fig. 16. The decomposed transfer function block of the bi-quad filter.

process for filter switching. In other words, before using the output from the filter, using the controller output to 'warm-up' the filter at first can be helpful. For identifying the length of the buffer setup process, a concept of the settling time constant is needed. From **Fig. 16**, the transfer function of the bi-quad filter can be split into two parts. The module above is a constant unit, while the lower part contains a typical second-order function and a differentiation element. Here, to simplify the calculation, the settling time ($\pm1\%$) of the typical second-order transfer function is used as the entire bi-quad filter's buffer time. According to the classic control theory, there are three types of second-order systems, including underdamped, overdamped, and critical damping systems.

As for the first type, underdamped system, its step response function $Y_1(t)$ can be given as

$$Y_1\left(t\right) = 1 - \frac{e^{-\xi\omega_b t}}{\sqrt{1-\xi^2}}\sin\left(\omega_d t + \varphi\right), \quad 0<\xi<1 \qquad (38)$$

in which, $\zeta = k_1/2 = b_b / (2\omega_b)$, $\omega_d = \omega_b (1 - \zeta^2)^{0.5}$, and $\varphi =$ arccos(ζ).

IEEE POWER ELECTRONICS REGULAR PAPER/LETTER/CORRESPONDENCE

According to the envelope of (38) and the $\pm 1\%$ error boundary, the settling time can be calculated as

$$1 \pm \frac{e^{-\xi \omega_b t}}{\sqrt{1-\xi^2}} = 1 \pm 0.01 \qquad (39)$$

$$T_b = \frac{-\ln(0.01) - \ln\sqrt{1-\xi^2}}{\xi \omega_b} \qquad (40)$$

For the overdamped system, the settling time is equal to the rising time, and its step response function $Y_2(t)$ can be expressed as

$$Y_2(t) = 1 - \frac{e^{-\left(\xi - \sqrt{\xi^2-1}\right)\omega_b t}}{2\sqrt{\xi^2-1}\left(\xi - \sqrt{\xi^2-1}\right)} + \frac{e^{-\left(\xi + \sqrt{\xi^2-1}\right)\omega_b t}}{2\sqrt{\xi^2-1}\left(\xi + \sqrt{\xi^2-1}\right)}, \quad \xi > 1 \quad (41)$$

Because it is hard to solve the settling time of (41) directly, the larger settling time of the subparts in the right is selected as the equivalent settling time, and it can be given as

$$\begin{cases} \left| \dfrac{e^{-\left(\xi - \sqrt{\xi^2-1}\right)\omega_b t}}{2\sqrt{\xi^2-1}\left(\xi - \sqrt{\xi^2-1}\right)} \right| = 0.01 \\[4mm] \left| \dfrac{e^{-\left(\xi + \sqrt{\xi^2-1}\right)\omega_b t}}{2\sqrt{\xi^2-1}\left(\xi + \sqrt{\xi^2-1}\right)} \right| = 0.01 \end{cases} \qquad (42)$$

$$\begin{cases} T_{b1} = \dfrac{-\ln(0.01) - \ln\left(2\sqrt{\xi^2-1}\left(\xi - \sqrt{\xi^2-1}\right)\right)}{\left(\xi - \sqrt{\xi^2-1}\right)\omega_b} \\[5mm] T_{b2} = \dfrac{-\ln(0.01) - \ln\left(2\sqrt{\xi^2-1}\left(\xi + \sqrt{\xi^2-1}\right)\right)}{\left(\xi + \sqrt{\xi^2-1}\right)\omega_b} \end{cases} \qquad (43)$$

Thus, T_b of the overdamped system can be given as

$$T_b = \max\{T_{b1}, T_{b2}\} = T_{b1} \qquad (44)$$

The step response of the third system, the critical damping system, $Y_3(t)$, can be given as

$$Y_3(t) = 1 - e^{-\omega_b t}\left(1 + \omega_b t\right), \quad \xi = 1 \qquad (45)$$

However, because of the existence of the transcendental equation, (45) and its derivative cannot be solved directly. For this situation, a small adjustment of the b_b can change the system to underdamped or overdamped systems.

According to (40), (43), and (44), the final expression of T_b can be given as

$$T_b = \begin{cases} \dfrac{-\ln(0.01) - \ln\sqrt{1-\xi^2}}{\xi \omega_b}, & 0 < \xi \leq 1 \\[5mm] \dfrac{-\ln(0.01) - \ln\left(2\sqrt{\xi^2-1}\left(\xi - \sqrt{\xi^2-1}\right)\right)}{\left(\xi - \sqrt{\xi^2-1}\right)\omega_b}, & 1 < \xi \end{cases} \qquad (46)$$

Then, the number of warm-up periods W for the bi-quad filter can be given as
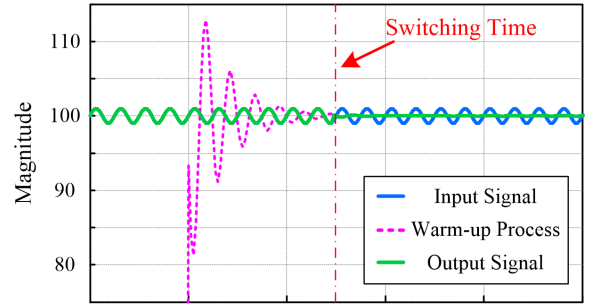

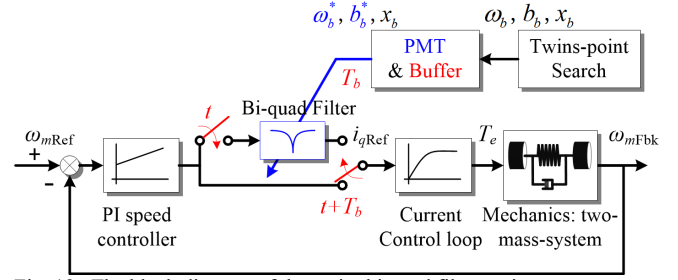Fig. 17. The performance of the bi-quad filter warm-up strategy.

Fig. 18. The block diagram of the entire bi-quad filter tuning strategy.

$$W = \lceil T_b / T_s \rceil \qquad (47)$$

For example, **Fig. 17** shows the performance of the bi-quad filter warm-up strategy. The input signal $X_{test}(t) = 100 + \sin(2\pi \times 200t)$. As for parameters of the bi-quad filter, $\omega_b = 2\pi \times 200$ rad/s, $b_b = 2\pi \times 50$ rad/s, $x_b = -30$ dB, and $T_s = 5e\text{-}4$ s. The vibration output at the beginning (the pink line) is avoided because of the warm-up process. In detail, the output of the bi-quad filter during the warm-up process (the first W sampling periods, in this case, $W = 59$) is not used. Hence, the real output of the bi-quad filter is always smooth.

The entire block diagram of the proposed modified bi-quad filter strategy is shown in **Fig. 18**. ω_{mRef} and i_{qRef} are the motor speed and q-axis current references. Moreover, the ω_{mFbk} and T_e are the motor speed feedback and electromagnetic torque. When the 'twins-point search' is finished, the 'PMT and buffer' block will calculate the corrected filter parameters and set the buffer time of the bi-quad filter switching.

V. EXPERIMENTAL RESULTS

The experimental setup is shown in **Fig. 19**, in which two TAMAGAWA TS4614N7680 servo motors are used as the drive and the load, respectively, and an elastic shaft connects them. Two motors are fed by one Zynq based servo drive, and they are equipped with 17-bit optical encoders. The detailed parameters of the servo drive system and controller are presented in Table I (the coefficients and factors from q_1 to q_5 can be fixed as the values in Table I in different situations). The random access memory (RAM) of the Zynq was extended to 1 GB by adding an external memory chip to record experimental data. Because the coupling of the motor 1 and motor 2 is different, using a different motor as the drive side can achieve different control performance and change the system characteristic. In most of the experiments, the motor 2 is the drive side, except a part of the twins-point search.
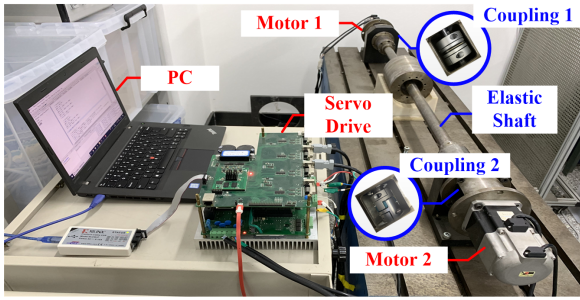
IEEE POWER ELECTRONICS REGULAR PAPER/LETTER/CORRESPONDENCE

Fig. 19. The experimental platform for the filter testing.

TABLE I: MAIN PARAMETERS OF THE SYSTEM

Parameter	Value
Motor Power P_N	750 W
Nominal Torque T_{eN}	2.39 N·m
Nominal Speed ω_N	3000 r/min
Nominal Current I_N	5×1.414 A
System Total Inertia J_{sum}	2.32e-3 kg·m²
Speed Control Frequency f_{ASR}	500 Hz
Threshold Coefficient q_1	0.8
Threshold Coefficient q_2	60 Hz
Threshold Coefficient q_3	20
Tuning Factor q_4	2.0
Tuning Factor q_5	5.0

A. The Resonance Characteristic Identification

1) The On-Line Identification and the Frequency Deviation

As shown in **Fig. 20**, according to the on-line FFT analysis, the oscillation frequency of the original unstable system f_{osc} is 176 Hz. For the conventional on-line method, this oscillation frequency is the notch frequency f_b. However, because the dominant cluster in the frequency spectrum is narrow, the notch bandwidth and the notch depth are hard to pick, which is one disadvantage of the on-line method. In **Fig. 20**, bi-quad filters with f_b = 176 Hz, x_b = -40 dB, and different notch bandwidths b_b are added to the system in the 2nd s. As mentioned in Part II, because of the oscillation frequency deviation [25]-[27], the bi-quad filters fail to make the system stable, and new oscillation frequencies appear (160 Hz, 149 Hz, 140 Hz). In this situation, the conventional on-line method will choose to expand the notch bandwidth, add new bi-quad filters, or change a new notch frequency. **Fig. 21** shows the oscillation frequency deviation trend of the system with different f_{ASR} and bi-quad filters. When f_{ASR} = 0.5 kHz, 1 kHz, and 2 kHz, the original oscillation frequency and the notch frequency of the system (represented by $b_b/\omega_b = 0$) are 176 Hz, 200Hz, and 271 Hz, respectively. $m(f_{osc})$ means the oscillation magnitude. For the same system, the frequency deviation phenomenon becomes worse with the increase of the speed loop control frequency f_{ASR}. Especially if the oscillation frequency becomes much higher than the real resonant frequency (f_r=167 Hz), this phenomenon will lead to a long
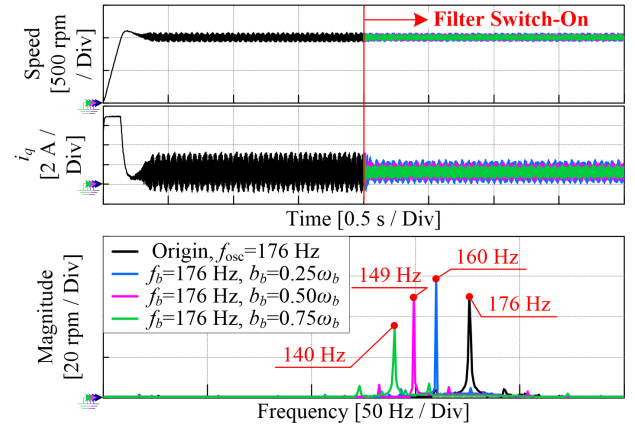

Fig. 20. The on-line identification based bi-quad filter performance and the speed feedback signals FFT results.
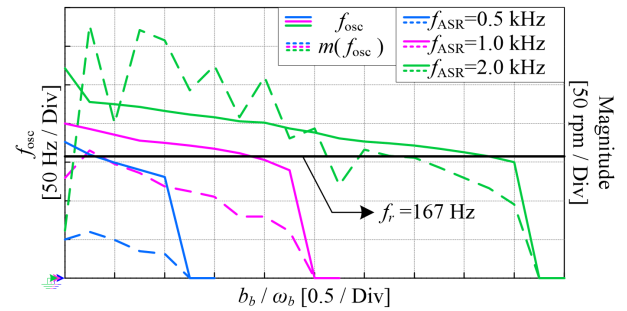

Fig. 21. The summarization of the oscillation frequency and magnitude of the system with different f_{ASR} and bi-quad filters.

adjustment process or even the failure of the on-line method. For example, in **Fig. 21**, when f_{ASR} = 2 kHz, the system's original oscillation frequency is 271 Hz. Then, to make the system stable, the bi-quad filter's notch bandwidth b_b has to increase to even 4.75 times larger than ω_b (2π×1287.25 rad/s).

2) The Twins-Point Search

Fig. 22 shows the twins-point search results. In **Fig. 22 (a)**, motor 1 is set as the drive side, and f_{ASR} = 4 kHz. 4096 points and 1.024 seconds classic chirp signal is used for the off-line resonant frequency identification. The magnitude of the chirp signal is $0.5I_N$, and the start and end frequencies of the signal are 30 Hz and 2000 Hz. The FFT result of the speed feedback is $m(f)$, and the twins-point search range is from 60 Hz to 1600 Hz. The purple line and the green line represent the changing process of the register values of the anti-resonant frequency f_{ar} and the resonant frequency f_r. During the searching process, experiment results show that two correct resonant frequencies (the black line, 535 Hz and 712 Hz) are successfully obtained by the proposed twins-point search. Additionally, in **Fig. 22 (b)**, motor 1 is the load side, while motor 2 is used as the drive, and f_{ASR} = 500 Hz. 1024 points and 2.048 seconds chirp signal with magnitude is $0.25I_N$ is chosen as the current reference. After one turn of the data traversal, the twins-point search finds a dominant resonant frequency of 167 Hz.

In the following experiments, for better verification of PMT, the platform and the program setting are the same as the **Fig. 22 (b)**, and the bi-quad filter factors are calculated as: $f_b = \omega_b /$
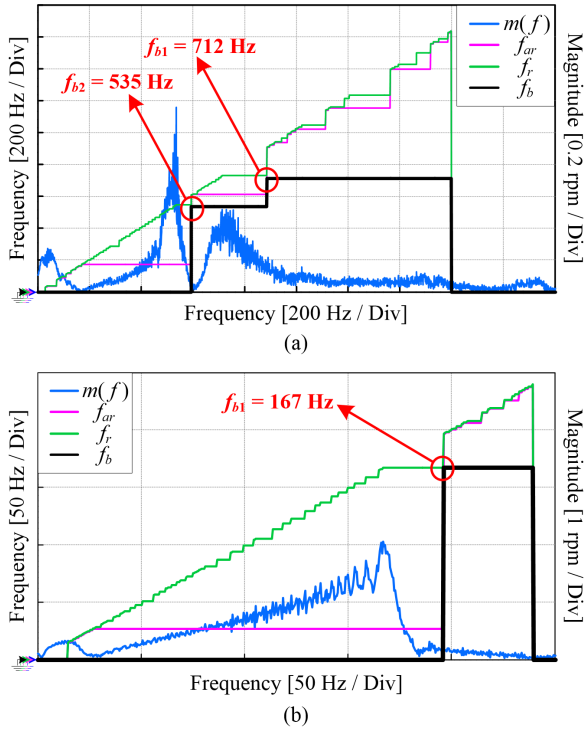
IEEE POWER ELECTRONICS REGULAR PAPER/LETTER/CORRESPONDENCE

Fig. 22. The process of the twins-point search. (a) Motor 1 is the drive side, f_{ASR} = 4 kHz. (b) Motor 2 is the drive side, f_{ASR} = 500 Hz.

2π = 167 Hz, b_b = (167 - 27)$\times 2 \times 2\pi$ rad/s = 280$\times 2\pi$ rad/s, x_b = -29.05 dB based on (3).

B. The Resonance Damping Test of PMT

To prove the effectiveness of PMT, several same chirp current signals that have been filtered by different bi-quad filters are injected into the system. **Fig. 23** shows FFT analysis results of the filtered current references and corresponding speed feedbacks. The expected notch frequency is 167 Hz, but the real notch frequency of the classic Tustin transformation based bi-quad filter (the blue line) deviates to 131 Hz. As for the PWT method (the purple line) and the ZPM method (the brown line), although their notch frequency is correct, their -3 dB rejection bandwidth shrinks or deviates sharply. Only the proposed PMT method (the green line), both the notch frequency and the bandwidth, are very close to the expected values (f_b = 167 Hz, b_b = 280$\times 2\pi$ rad/s), and the stimulated speed feedback analysis results can also verify this point. Additionally, in this case, because of $b_b > \pi f_s$, the conventional notch filter is unstable.

Next, the comparison results of PWT, ZPM, and PMT under a nominal switching torque are shown in **Fig. 24**. According to the tuning process in [2], when the expected speed-loop bandwidth f_{sc} of the original system (without filter) is increased to 5 Hz, the system becomes unstable. As for the PWT based bi-quad filter, when f_{sc} is increased to 7 Hz, the system also becomes unstable. The ZPM based bi-quad filter has better performance, but its stable gain limit is still only 10 Hz. However, in the precondition of stability, the system's bandwidth with the PMT-based bi-quad filter can be increased
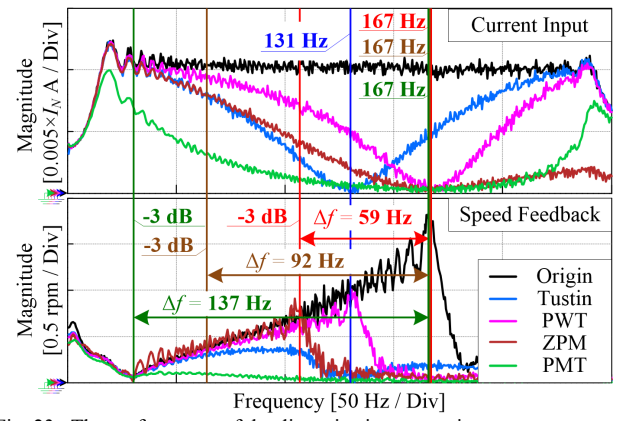

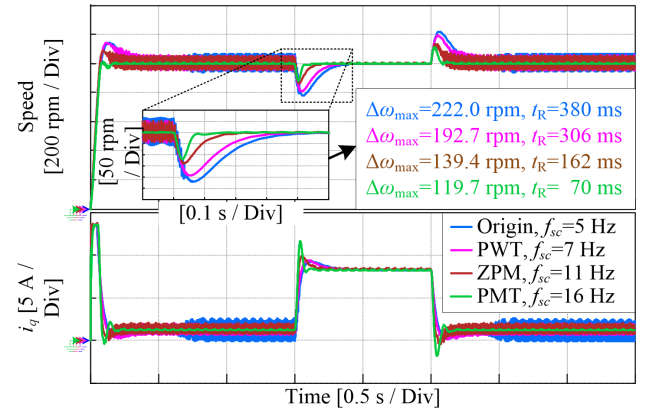Fig. 23. The performance of the discretization correction.

Fig. 24. The comparison result of PWT, ZPM, and PMT based bi-quad filters with a nominal switching torque.
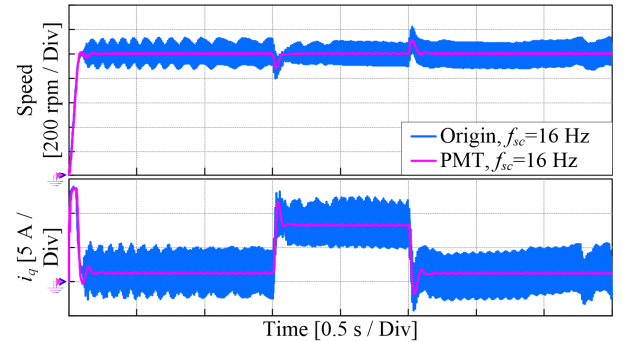
Fig. 25. The performance of the system with and without PMT based bi-quad filter.

to 16 Hz (it is still not the maximum bandwidth), which is triple times of the bandwidth of the original system. PMT also has a smaller maximum speed drop $\Delta\omega_{max}$ and a shorter recovery time t_R than the original system, the PWT method, and the ZPM method. Besides, **Fig. 25** shows the performance of the system with and without the PMT based bi-quad filter. When f_{sc} of the original system is also increased to 16 Hz, a severe oscillation happens.

Additionally, the motor side and the load side speed feedback signals are shown in **Fig. 26** (PMT, f_{sc} is 16 Hz). The system is stable, and the dominant residual frequency of the speed ripple is rotating frequency (16.67 Hz), which is caused by the slight mechanical installation misalignment.

Furthermore, the stable maximum speed-loop bandwidths of the PWT, ZPM and PMT based bi-quad filters with variable parameters are recorded in Table II (f_b = 167 Hz, b_b = 280×2π rad/s, x_b = -29.05 dB). As mentioned above, the maximum bandwidth of the system without the filter is 4 Hz. According to Table II, the decrease of f_b and the narrowing of b_b have a larger influence on the filter and will reduce the maximum bandwidth of the system in this situation. Because PMT does not change the filter's basic characteristic, the bi-quad filter is still sensitive to the parameter variation as before. However, compared with PWT and ZPM, the proposed PMT method can help the classic bi-quad filter accomplish its duty better and reach higher maximum bandwidth in the same case.

C. The Verification of the Filter Buffer Strategy

In the buffer experiment, the system's speed loop is regulated to the state with a constant nominal torque, and its bandwidth is 4 Hz. All of the initial values of filter variables are set to zero. According to (47), the amount of the warm-up period of the filter W is 3. The performances of the system with and without the buffer strategy are shown in **Fig. 27**. A transient state oscillation (caused by unbuffered bi-quad filter switching) happens (the maximum speed drop $\Delta\omega_{max}$ is 22 rpm, and the recovery time t_R is 148 ms). In contrast, the bi-quad filter with the buffer strategy, the purple line, has a smoother transient process. The influences from the switching and initial values of the filter have been reduced significantly ($\Delta\omega_{max}$ = 9 rpm, t_R = 80 ms). Because of the notch bandwidth deviation phenomenon analyzed in (36), the settling time of the used digital filter used does not perfectly match the original continuous bi-quad filer. Hence, the speed and current jitters are not totally eliminated. Considering the reverse discretization calculation process is complex and the transient performance has been improved, the further correction of the settling time is not discussed in this paper.

VI. Conclusion

This paper has proposed three simple and useful modification methods to improve the identification, discretization, and switching process of the classic bi-quad filter tuning in the industrial servo drive system. Firstly, in order to avoid the oscillation frequency deviation phenomenon of the on-line identification and the information loss of the classic off-line based maximum point search method, a twins-point search method is presented to achieve a comprehensive system diagnosis and obtain accuracy filter factors. Next, a parameter mapping Tustin method is proposed to solve the characteristic distortion problem caused by the classic Tustin, pre-warped Tustin, and zero-pole matching methods and realize an accurate discretization of the bi-quad filter. Analysis and experimental results show that the proposed parameter mapping Tustin method has better discretization performance and resonance damping ability. Furthermore, considering the filter's unbuffered switching can lead to jitter and vibration, a buffer strategy is used to make the bi-quad filter switching process smoother and independent of its initial values. Besides, these three sub-methods can be used separately in other filter-
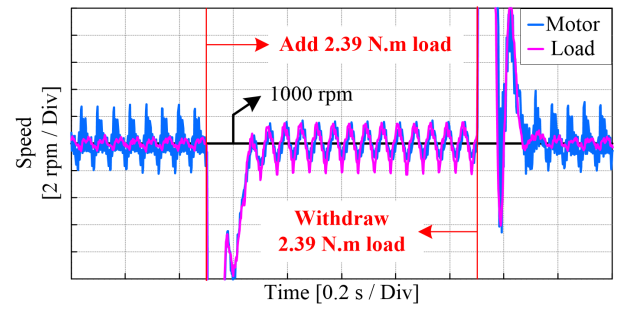

Fig. 26. The motor side and the load side speed feedback signals of PMT.

TABLE II: THE STABLE MAXIMUM SPEED-LOOP BANDWIDTHS OF PWT, PMT, AND ZPM WITH THE PARAMETER VARIATION (UNIT: HZ)

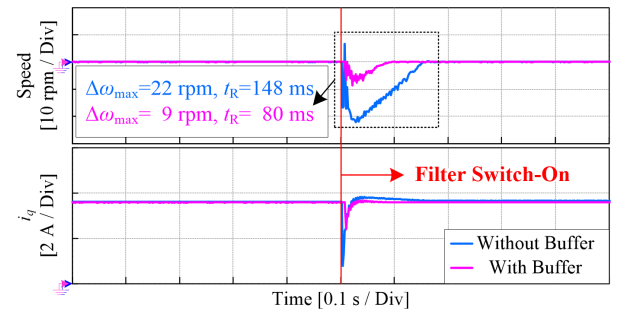| f_b	80%	90%	100%	110%	120%
PWT	18	18	18	10	8
PMT	6	6	6	3	4
ZPM	9	10	10	6	5
b_b	80%	90%	100%	110%	120%
PWT	9	14	18	18	18
PMT	6	6	6	6	7
ZPM	8	10	10	11	11
x_b	80%	90%	100%	110%	120%
PWT	18	18	18	18	18
PMT	6	6	6	6	6
ZPM	10	10	10	10	10

Fig. 27. The performance of the buffer strategy.

related algorithms. The proposed modified bi-quad filter tuning strategy's effectiveness and advantages are verified on an elastic coupling permanent magnet synchronous motor platform.

References

[1] C. Hsu, and Y. Lai, "Novel online optimal bandwidth search and autotuning techniques for servo motor drives," *IEEE Trans. Ind. Appl.*, vol. 53, no. 4, pp. 3635–3642, Jul/Aug. 2017.

[2] Y. Chen, M. Yang, J. Long, W. Qu, D. Xu, and F. Blaabjerg, "A moderate on-line servo controller parameter self-tuning method via variable-period inertia identification," *IEEE Trans. Power Electron.*, vol. 34, no. 12, pp. 12165–12180, Dec. 2019.

[3] G. Ellis, and R.D. Lorenz, "Resonant load control methods for industrial servo drives," in *Proc. IAS*, 2000, pp. 1438–1445.

[4] G. Ellis, and Z. Gao, "Cures for low-frequency mechanical resonance in industrial servo systems," in *Proc. IAS*, 2001, pp. 1–7.

[5] E. Fuentes, D. Kalise, and R. M. Kennel, "Smoothened Quasi-Time-Optimal Control for the Torsional Torque in a Two-Mass System," *IEEE Trans. Ind. Electron.*, vol. 63, no. 6, pp. 3954–3963, Jun. 2016.

[6] K. Szabat and T. Orlowska-Kowalska, "Application of the Kalman filters to the high-performance drive system with elastic coupling," *IEEE Trans. Ind. Electron.*, vol. 63, no. 6, pp. 4226–4235, Nov. 2012.

IEEE POWER ELECTRONICS REGULAR PAPER/LETTER/CORRESPONDENCE

[7] K. Szabat, T. Tran-Van, and M. Kami´nski, "A modified fuzzy Luenberger observer for a two-mass drive system," *IEEE Trans. Ind. Informat.*, vol. 11, no. 2, pp. 531–539, Apr. 2015.

[8] S. Thomsen, N. Hoffmann, and F. W. Fuchs, "PI control, PI-based state space control, and model-based predictive control for drive systems with elastically coupled loads—A comparative study," *IEEE Trans. Ind Electron.*, vol. 58, no. 8, pp. 3647–3657, Aug. 2011.

[9] S. E. Saarakkala, and M. Hinkkanen, "State-space speed control of two-mass mechanical systems: analytical tuning and experimental evaluation," *IEEE Trans. Ind. Appl.*, vol. 50, no. 5, pp. 3428–3437, Sept/Oct. 2014.

[10] X. Li, W. Zhou, J. Luo, J. Qian, W. Ma, P. Jiang, and Y. Fan, "A new mechanical resonance suppression method for large optical telescope by using nonlinear active disturbance rejection control," *IEEE Access*, vol. 7, pp. 94400–94414, Jul. 2019.

[11] K. Szabat, T. Orlowska-Kowalska, and M. Dybkowski, "Indirect Adaptive Control of Induction Motor Drive System With an Elastic Coupling," *IEEE Trans. on Ind. Electron.*, vol. 56, no. 10, pp. 4038-4042, Oct. 2009.

[12] M. Calvini, M. Carpita, A. Formentini and M. Marchesoni, "PSO-based self-commissioning of electrical motor drives," *IEEE Trans. Ind. Electron.*, vol. 62, no. 2, pp. 768-776, Feb. 2015.

[13] S. Yang, and S. Wang, "The Detection of Resonance Frequency in Motion Control Systems," *IEEE Trans. Ind. Appl.*, vol. 50, no. 5, pp. 3423–3427, Sept/Oct. 2014.

[14] D. -H. Lee, J. H. Lee, and J. -W. Ahn, "Mechanical vibration reduction control of two-mass permanent magnet synchronous motor using adaptive notch filter with fast Fourier transform analysis," *IET Electric Power Appl.*, vol. 6, no. 7, pp. 455–461, Aug. 2012.

[15] J. Kang, S. Chen, and X. Di, "Online detection and suppression of mechanical resonance for servo system," in *Proc. ICICIP*, 2012, pp. 16–21.

[16] Y. Chen, M. Yang, Y. Sun, J. Long, D. Xu, and F. Blaabjerg, "A modified full-band adjustable bi-quad filter for mechanical resonance suppression in industrial servo drive systems," in *Proc. IAS*, 2019, pp. 1–6.

[17] Y. Wang, Q. Zheng, H. Zhang, and Z. Du, "A study on the acceleration optimization control method for the integrated helicopter engine system based on torsional vibration suppression," *IEEE Access*, vol. 7, pp. 1182–1194, Dec. 2018.

[18] D. Yazdani, A. Bakhshai, G. Joos and M. Mojiri, "A nonlinear adaptive synchronization technique for grid-connected distributed energy sources," *IEEE Trans. Power Electron.*, vol. 23, no. 4, pp. 2181-2186, Jul. 2008.

[19] B. Singh, C. Jain, S. Goel, A. Chandra, and K. Al-Haddad, "A multifunctional grid-tied solar energy conversion system with ANF-based control approach," *IEEE Trans. Ind. Appl.*, vol. 52, no. 5, pp. 3663–3672, Sept/Oct. 2016.

[20] R. S. R. Chilipi, N. A. Sayari, K. H. A. Hosani, and A. R. Beig, "Adaptive notch filter-based multipurpose control scheme for grid-interfaced three-phase four-wire DG inverter," *IEEE Trans. Ind. Appl.*, vol. 53, no. 4, pp. 4015–4027, Jul/Aug. 2017.

[21] P. Rodríguez, A. Luna, I. Candela, R. Mujal, R. Teodorescu and F. Blaabjerg, "Multiresonant frequency-locked loop for grid synchronization of power converters under distorted grid conditions," *IEEE Trans. on Ind. Electron.*, vol. 58, no. 1, pp. 127-138, Jan. 2011.

[22] J. Wang, J. D. Yan, L. Jiang and J. Zou, "delay-dependent stability of single-loop controlled grid-connected inverters with LCL filters," *IEEE Trans. Power Electron.*, vol. 31, no. 1, pp. 743-757, Jan. 2016.

[23] R. Peña-Alzola, M. Liserre, F. Blaabjerg, M. Ordonez and Y. Yang, "LCL-filter design for robust active damping in grid-connected converters," *IEEE Trans. Ind. Informat.*, vol. 10, no. 4, pp. 2192-2203, Nov. 2014.

[24] W. Yao, Y. Yang, X. Zhang, F. Blaabjerg, and P. C. Loh, "Design and analysis of robust active damping for LCL filters using digital notch filters," *IEEE Trans. Power Electron.*, vol. 32, no. 3, pp. 2360–2375, Mar. 2016.

[25] W. Wang, J. Xu and A. Shen, "Detection and reduction of middle frequency resonance for industrial servo," in *Proc. ICIST*, 2012, pp. 153-160.

[26] Y. Chen, M. Yang, K. Hu, D. Xu and F. Blaabjerg, "Suppression of mechanical resonance in digital servo system considering oscillation frequency deviation," in *Proc. IECON*, 2017, pp. 2201-2206.

[27] Y. Chen, M. Yang, J. Long, K. Hu, D. Xu, and F. Blaabjerg, "Analysis of oscillation frequency deviation in elastic coupling digital drive system and robust notch filter strategy," *IEEE Trans. Ind. Electron.*, vol. 66, no. 1, pp. 90–101, Jan. 2019.

[28] S. E. Saarakkala, and M. Hinkkanen, "Identification of two-mass mechanical systems using torque excitation: design and experimental evaluation," *IEEE Trans. Ind. Appl.*, vol. 51, no. 5, pp. 4180–4189, Sept/Oct. 2015.

[29] S. Villwock, and M. Pacas, "Application of the Welch-method for the identification of two- and three-mass-systems," *IEEE Trans. Ind. Electron.*, vol. 55, no. 1, pp. 457–466, Jan. 2008.

[30] Z. Henning, and M. Pacas, "Encoderless identification of two-mass-systems utilizing an extended speed adaptive observer structure," *IEEE Trans. Ind. Electron.*, vol. 64, no. 1, pp. 595–604, Jan. 2016.

[31] C. Kang, and C. Kim, "An adaptive notch filter for suppressing mechanical resonance in high track density disk drives," *Microsystem Technologies*, vol. 11, pp. 638–652, May 2005.

[32] K. Hirano, S. Nishimura, and S. K. Mitra, "Design of digital notch filters," *IEEE Trans. Circuits Syst.*, vol. 21, no. 4, pp. 540-546, Jul. 1974.

Yangyang Chen (S'19) received the B.S. degree in electrical engineering in 2016 from Harbin Institute of Technology, Harbin, China, where he is currently working toward the Ph.D. degree in power electronics and electrical drives in the School of Electrical Engineering and Automation.

His current research interests include multi-axis servo systems, mechanical resonance and control parameter self-tuning strategy.

Ming Yang (M'14–SM'18) received the B.S. and M.S. and Ph.D. degrees in Electrical Engineering from Harbin Institute of Technology (HIT), Harbin, China, in 2000, 2002 and 2007, respectively.

In 2004, he joined as a Lecturer with the Department of Electrical Engineering, HIT, where he has been a Professor of Electrical Engineering since 2015. From 2009 to 2012, he was a Postdoctoral Fellow with Shanghai STEP Electric Corporation. He has authored more than 40 technical papers published in journals and conference proceedings. He is the holder of 14 Chinese patents. His current major research interests include PMSM servo systems, predictive current control and mechanical resonance suppression.

Yongping Sun received the M.S. degree in mechanical engineering in 2014 from Harbin Institute of Technology, Harbin, China. He is currently working toward the Ph.D. degree in power electronics and electrical drives with the School of Electrical Engineering and Automation, Harbin Institute of Technology, Harbin, China.

His current research interests include multi-axis servo systems, vibration suppression, and high-precision mechanical servo systems.

IEEE POWER ELECTRONICS REGULAR PAPER/LETTER/CORRESPONDENCE

Jiang Long received the M.S. degree in power electronics and electrical drives in 2015, from the Harbin University of Science and Technology, Harbin, China. He is currently working towards Ph.D. degree in power electronics and electrical drives with the School of Electrical Engineering and Automation of Harbin Institute of Technology.

His current research interests include on PMSM servo systems, predictive current control and parameter identification.

Dianguo Xu (M'97–SM'12–F'17) received the B.S. degree in Control Engineering from Harbin Engineering University, Harbin, China, in 1982, and the M.S. and Ph.D. degrees in Electrical Engineering from Harbin Institute of Technology (HIT), Harbin, China, in 1984 and 1989, respectively.

In 1984, he joined the Department of Electrical Engineering, HIT, as an Assistant Professor. Since 1994, he has been a Professor in the Department of Electrical Engineering, HIT. He was the Dean of the School of Electrical Engineering and Automation, HIT, from 2000 to 2010. He is currently the Vice President of the HIT. His research interests include renewable energy generation, power quality mitigation, sensorless motor drives, and high performance servo systems.

Dr. Xu is an Associate Editor of the IEEE TRANSACTIONS ON INDUSTRIAL ELECTRONICS.

Frede Blaabjerg (S'86–M'88–SM'97–F'03) received the Ph.D. degree in electrical engineering from Aalborg University, Aalborg, Denmark, in 1992.

He was with ABB-Scandia, Randers, Denmark, from 1987 to 1988. He became an Assistant Professor in 1992, an Associate Professor in 1996, and a Full Professor of Power Electronics and Drives in 1998 with Aalborg University. His current research interests include wind turbines, PV systems, reliability, harmonics, and adjustable speed drives.

Dr. Blaabjerg was a recipient of 15 IEEE Prize Paper Awards, the IEEE PELS Distinguished Service Award in 2009, the IEEE William E. Newell Power Electronics Award 2014, and the Villum Kann Rasmussen Research Award 2014. He was an Editor-in-Chief of the IEEE TRANSACTIONS ON POWER ELECTRONICS from 2006 to 2012. He has been a Distinguished Lecturer for the IEEE Power Electronics Society from 2005 to 2007 and for the IEEE Industry Applications Society from 2010 to 2011. He was nominated in 2014 by Thomson Reuters to be among the most 250 cited researchers in engineering in the world.